

Chapter 2

Finite-element-model Updating Using Nelder–Mead Simplex and BFGS Methods

Abstract. This chapter presents the Nelder–Mead simplex method and the Broyden–Fletcher–Goldfarb–Shanno (BFGS) method for finite-element-model updating. The methods presented have been tested on a simple beam and an unsymmetrical H-shaped structure. It was noted that, on average, the Nelder–Mead simplex method gives more accurate results than did the BFGS method. This is mainly because the BFGS method requires the calculation of gradients, which is prone to numerical errors within the context of finite-element-model updating.

Keywords: Nelder–Mead, objective function, Broyden–Fletcher–Goldfarb–Shanno, reduction methods, expansion methods, Guyan reduction method

2.1 Introduction

In Chapter 1, the concept of finite-element-model updating was introduced. It was noted there that a model-updating process is essentially an optimization problem where the updating parameters are those parameters in the finite-element model that are deemed to be highly uncertain, while the objective function is some measure of the distance between the finite-element’s predicted data and measured data.

The purpose of this chapter is to introduce the concept of the updating of finite-element models using the Nelder–Mead (NM) simplex and Broyden–Fletcher–Goldfarb–Shanno (BFGS) optimization methods. The NM simplex method was used because it was found to be advantageous in that it (Olsson and Nelson, 1975):

- gives good results in the early stages of the simulations;
- does not require the use of the gradient and the Hessian of the objective function;
- is computationally efficient; and
- is relatively simple to understand and use.

The BFGS method was used because it has the following advantages. It preserves the necessary conditions for convergence – for example stability, descending direction, and positive definiteness (Azizi *et al.*, 2005). There is always a mismatch between the coordinates of the measured data and those of the finite-element model (Friswell and Mottershead, 1995). Because of this mismatch, it is always a good idea to reduce the system's matrices so that they correspond to the measured degrees of freedom, or to expand the measured coordinates so that they are of the same size as those from the finite-element model.

The purpose of this chapter is also to review reductions and expansions methods that equalize the size of the measured data and the system matrices of the structure in question. One question that is of great importance is: how do we compare the measurements and data from the finite-element model? This chapter reports an investigation that was carried out on how the data can be compared to establish whether the finite-element model has been sufficiently well updated.

The presented NM and BFGS optimization methods were then used for finite-element updating and were tested on a simple beam and an unsymmetrical H-shaped structure.

2.2 Introduction to Structural Dynamics

In this chapter, the modal properties *i.e.*, natural frequencies and mode shapes were used as a basis for finite-element-model updating. Thus, these parameters are described in this section. The modal properties are related to the physical properties of the structure. All elastic structures may be described in terms of their distributed mass, damping and stiffness matrices in the time domain through the following expression (Paz and Leigh, 2003):

$$[M]\{\ddot{X}\} + [C]\{\dot{X}\} + [K]\{X\} = \{F\} \quad (2.1)$$

where $[M]$ is the mass matrix, $[C]$ is the damping matrix, $[K]$ is the stiffness matrix, $\{X\}$ is the displacement vector, $\{\dot{X}\}$ is the velocity vector, $\{\ddot{X}\}$ is the acceleration vector, and $\{F\}$ is the applied force vector.

If Equation 2.1 is transformed into the modal domain to form an eigenvalue equation for the i th mode, then (Ewins, 1995):

$$(-\bar{\omega}_i^2[M] + j\bar{\omega}_i[C] + [K])\{\bar{\phi}\}_i = \{0\} \quad (2.2)$$

Here, $j = \sqrt{-1}$; $\bar{\omega}_i$ is the i th complex eigenvalue; and $\{0\}$ is the null vector. In Equation 2.2 the real part of $\{\bar{\phi}\}_i$ corresponds to the normalized mode shape $\{\phi\}_i$ while the imaginary part of $\bar{\omega}_i$ corresponds to the natural frequency ω_i .

From Equation 2.2 it may be deduced that the changes in the mass and stiffness matrices cause changes in the modal properties of the structure.

Therefore, the modal properties can be identified through the identification of the correct mass and stiffness matrices. The frequency-response function (FRF) is defined as the ratio of the Fourier-transformed response to the Fourier-transformed force. The FRF may be written in terms of the modal properties by using the modal summation equation as follows (Fu and He, 2001):

$$H_{kl}(\omega) = \sum_{i=1}^N \frac{-\omega^2 \phi_k^i \phi_l^i}{-\omega^2 + 2\zeta_i \omega_i \omega j + \omega_i^2} \quad (2.3)$$

In Equation 2.3 $H_{kl}(\omega)$ is an FRF due to excitation at position k and response measurement at position l , ω is the frequency point, ω_i is the i th natural frequency point, N is the number of modes and ζ_i is the damping ratio of mode i .

The excitation and response of the structure and Fourier-transform method (Ewins, 1995) can be used to calculate the FRF. Through Equation 2.3 and modal analysis (Ewins, 1995; Fu and He, 2001), the natural frequencies and mode shapes can be indirectly calculated from the FRFs. The modal properties of a dynamic system depend on the mass and stiffness matrices of the system as indicated by Equation 2.3. Therefore, the measured modal properties can be reproduced by the model if the correct mass and stiffness matrices are identified.

The finite-element-model updating process is achieved by identifying the correct mass and stiffness matrices. In the light of the measured data, the correct mass and stiffness matrices can be obtained by identifying the correct moduli of elasticity of various sections of the structure under consideration. In this chapter, to identify correctly the moduli of elasticity that would give the updated finite-element model, the following objective function that measures the distance between measured modal data and finite-element-model calculated modal data, was minimized (Marwala, 1997):

$$E = \left\| \sum_{i=1}^N [(-\omega_i^2 [M] + j\omega_i [C] + [K])\{\phi\}_i] \right\| \quad (2.4)$$

Here, N is the number of measured modes; E is the error; and $\| \cdot \|$ is the Euclidean norm.

In Equation 2.4 the mass, damping and stiffness matrices are obtained from the finite-element model, while the natural frequencies and mode shapes are measured. If the natural frequencies and mode shapes of the system are described by the mass, damping and stiffness matrices then E is equal to zero. Therefore, the minimization of E identifies the updated finite-element model. Thus, the process of finite-element-model updating may be viewed as being an optimization problem. The updated finite-element models of a simple beam and an unsymmetrical H-shaped structure that are identified in this chapter were evaluated by comparing the

natural frequencies and mode shapes from the finite-element models before and after updating to the measured ones.

2.3 Expansion/Reduction Methods

2.3.1 Model Expansion and Reduction Procedures

Two approaches may be pursued to ensure that the measured coordinates and modes are equal to the computed ones. These approaches are:

1. the experimental data may be expanded to the same number of degrees of freedom as the computed ones; and
2. the computed results may be reduced to the same number of coordinates as the measured ones.

Several techniques may be employed. As part of this study, the methods were implemented, and their effectiveness evaluated with respect to each method. The reduction methods applied were (Friswell and Mottershead, 1995):

- Guyan static reduction method;
- Guyan dynamic reduction method;
- Improved reduced system (IRS); and
- System equivalent reduction expansion process (SEREP).

The expansion methods applied were:

- expansion using mass and stiffness matrices; and
- expansion using modal data.

2.3.2 Model Reduction

A) Guyan Static Reduction (GSR) Method

This method was used to reduce the mass and stiffness matrices to the levels of the measured degrees of freedom. Prakash and Prabhu (1986) used the GSR method for reducing the mass and stiffness matrices in dynamic substructures, whereas Bushard (1981) applied this method to reduce system matrices in thermal problems. Bouhaddi and Fillod (1992) applied the GSR method for choosing master degrees of freedom in substructuring, while Häggblad and Eriksson (1993) applied the model condensation technique for analyses of large structures. Applications of reduction methods to nonlinear systems include Noor (1981).

In the GSR method, the state and force vectors, $\{x\}$ and $\{f\}$, and the mass and stiffness matrices $[M]$ and $[K]$ are partitioned into the measured (master) and unmeasured (slave) coordinates as follows (Friswell and Mottershead, 1995):

$$\begin{bmatrix} [M_{mm}] & [M_{ms}] \\ [M_{sm}] & [M_{ss}] \end{bmatrix} \begin{Bmatrix} \ddot{x}_m \\ \ddot{x}_s \end{Bmatrix} + \begin{bmatrix} [K_{mm}] & [K_{ms}] \\ [K_{sm}] & [K_{ss}] \end{bmatrix} \begin{Bmatrix} x_m \\ x_s \end{Bmatrix} = \begin{Bmatrix} f_m \\ 0 \end{Bmatrix} \quad (2.5)$$

Here, the subscripts m and s correspond to master and slave coordinates, respectively. The inertia terms are neglected to obtain the equation (Guyan, 1965):

$$[K_{sm}]\{x_m\} + [K_{ss}]\{x_s\} = [T_s]\{x_m\} \quad (2.6)$$

This equation may be used to eliminate the slave coordinate to leave the following equation (Guyan, 1965):

$$\begin{Bmatrix} x_m \\ x_s \end{Bmatrix} = \begin{bmatrix} [I] \\ -[K_{ss}]^{-1}[K_{sm}] \end{bmatrix} \{x_m\} = [T_s]\{x_m\} \quad (2.7)$$

The parameter T_s denotes the static transformation between full state vector and master coordinates and the parameter $[I]$ is the identity matrix. The reduced mass $[M_R]$ and stiffness $[K_R]$ matrices can be calculated as follows:

$$[M_R] = [T_s]^T [M] [T_s] \quad (2.8)$$

and

$$[K_R] = [T_s]^T [K] [T_s] \quad (2.9)$$

The frequency-response functions generated by the reduced-mass matrices are exact at zero frequency because the inertia matrices were neglected.

B) Guyan Dynamic Reduction (GDR) Method

The GSR method neglects the effects of inertia. However, the GDR method takes into account the inertia effect, assuming a particular frequency. Salvini and Vivio (2007) applied the GDR method to reduce the system matrices, while Yang (2009) applied it in model reduction using a Neumann series expansion. Yin *et al.* (2009) applied the GDR method to structural damage detection in a transmission tower. The technique used ambient vibration data.

The choice of frequency affects the accuracy of the reduced model. In the GDR method, the mass and stiffness matrices are partitioned into slave and master coordinates. The modified transformation matrices are as follows (Paz, 1984):

$$\begin{Bmatrix} \phi_m \\ \phi_s \end{Bmatrix} = \begin{bmatrix} [I] \\ -([K_{ss}] - \omega^2[M_{ss}])^{-1}([K_{sm}] - \omega^2[M_{sm}]) \end{bmatrix} \{\phi_m\} = [T_D] \{\phi_m\} \quad (2.10)$$

The dynamic transformation, $[T_D]$, may then be used in the same way as the static transformation, $[T_S]$, to obtain the reduced mass and stiffness matrices similar to Equations 2.8 and 2.9.

C) Improved Reduced System (IRS)

The IRS is an improvement of the Guyan static reduction method. This method uses the transformation, the reduced mass and stiffness matrices from the Guyan reduction method together with the $[S]$ matrix, which is made out of zeros and the inverse of the slave partition of the stiffness matrix, to obtain a new transformation matrix (O'Callahan, 1989):

$$[T] = \begin{bmatrix} [I] \\ -[K_{ss}]^{-1}[K_{sm}] \end{bmatrix} + [S][M][S][M_R]^{-1}[K_R] \quad (2.11)$$

where

$$[S] = \begin{bmatrix} [0][0] \\ [0][K_{ss}]^{-1} \end{bmatrix} \quad (2.12)$$

Friswell *et al.* (1995) studied the convergence of the iterated IRS method, whereas Kim and Cho (2008) studied the subdomain optimization of a multi-domain structure built by the IRS reduced system. Li *et al.* (2008) refined reduced models of dynamic systems, while Xia and Lin (2004) improved the iterated IRS method and applied this to structural eigensolutions. Friswell *et al.* (1998) developed iterated IRS techniques in structural dynamics. The iterated IRS method converges to the same transformation as the SEREP, which is the subject of the next section.

D) System Equivalent Reduction Expansion Process (SEREP)

The system equivalent reduction expansion process (SEREP) (O'Callahan *et al.*, 1989) partitions the analytical mode shapes into measured and unmeasured coordinates, and obtains the transformation by multiplying that with the generalized pseudo-inverse. See Equations 2.13 and 2.14.

$$[\phi] = \begin{bmatrix} \phi_m \\ \phi_s \end{bmatrix} \quad (2.13)$$

$$[T_U] = \{\phi\}\phi^+ \quad (2.14)$$

where

$$\phi^+ = (\phi_m^T \phi_m)^{-1} \phi_m^T \quad (2.15)$$

The transformation may then be used in the same way as the static transformation, $[T_S]$, to obtain the reduced mass and stiffness matrices similar to Equations 2.8 and 2.9. Das and Dutt (2008) used the SEREP to reduce the model of a rotor-shaft system, while Sastry *et al.* (2003) introduced an iterative SEREP for extracting the high-frequency response.

2.3.3 Model Expansion

A) Expansion Using Mass and Stiffness Matrices (EMS)

In essence, this method is the inverse of the Guyan reduction method. Suppose ω_{mj} and ϕ_{mj} are the measured natural frequencies and mode shapes of coordinates i . Then the mass and the stiffness matrices from the finite-element analysis may be partitioned into measured and unmeasured coordinates. The equation of motion may then be written as follows (Friswell and Mottershead, 1995):

$$\left(-\omega_{mj}^2 \begin{bmatrix} [M_{mm}] & [M_{ms}] \\ [M_{sm}] & [M_{ss}] \end{bmatrix} + \begin{bmatrix} [K_{mm}] & [K_{ms}] \\ [K_{sm}] & [K_{ss}] \end{bmatrix} \right) \begin{Bmatrix} \phi_{mj} \\ \phi_{sj} \end{Bmatrix} = \begin{Bmatrix} 0 \\ 0 \end{Bmatrix} \quad (2.16)$$

where ϕ_{sj} represents the mode shape at the slave or the unmeasured coordinates. Rearranging the lower part of the matrix equation produces a solution for the unknown part of the measured mode shape vector. Thus (Friswell and Mottershead, 1995):

$$\{\phi_{sj}\} = -(-\omega_{mj}^2 [M_{ss}] + [K_{ss}])^{-1} (-\omega_{mj}^2 [M_{sm}] + [K_{sm}]) \{\phi_{mj}\} \quad (2.17)$$

Other estimates of the unmeasured degrees of freedom may be obtained by using the upper part of Equation 2.12, which will involve the pseudo inverse. Using the upper part is satisfactory if the number of measured degrees of freedom exceeds

the number of unmeasured degrees of freedom. Similarly, the unmeasured FRF may be calculated using the following equation (Friswell and Mottershead, 1995):

$$[H_{sj}] = -(-\omega_{mj}^2[M_{ss}] + [K_{ss}])^{-1}(-\omega_{mj}^2[M_{sm}] + [K_{sm}])\{H_{mj}\} \quad (2.18)$$

Corus *et al.* (2006) applied this technique to improve structural dynamics models, while Kammer and Peck (2008) applied the expansion technique for sensor placement and Kammer (2005) applied this method for improved modal vibration testing.

B) Expansion Using Modal Data (EMD)

This method uses the modal data obtained from the finite-element model to estimate the modes at the unmeasured degrees of freedom. The measured modes are assumed to be a linear combination of the analytical modes at measured degrees of freedom and a transformation, T , as indicated by the following equation (Friswell and Mottershead, 1995):

$$\{\phi_m\} = [\phi_a]_m [T] \quad (2.19)$$

where $[\phi_a]_m$ represents the analytical mode shapes at measured degrees of freedom. Applying the pseudo-inverse to Equation 2.19 gives the transformation as (Friswell and Mottershead, 1995):

$$[T] = [\phi_a]_m^+ \{\phi_m\} \quad (2.20)$$

where $+$ indicates the pseudo-inverse. This transformation may be used to estimate the modes at unmeasured degrees of freedom from the finite-element analysis. It may also be used to smooth out the measured modes. Thus (Friswell and Mottershead, 1995):

$$\{\phi_m\}_{smoothed} = [\phi_a]_m [T] \quad (2.21)$$

$$[\phi_s] = [\phi_a]_m [T] \quad (2.22)$$

where $[\phi_a]_m$ represents the analytical mode shapes at the unmeasured degrees of freedom. The transformation may be obtained by using only the analytical modal data or the combination of measured and analytical data. This method is like an inverse of the SEREP method.

Marwala (1997) compared these methods and found that the reduction methods are more reliable than the expansion methods. This is because the expansion

methods are more computationally intensive when compared to the reduction methods. Furthermore, the SEREP method was found to be susceptible to numerical instability. The IRS was found to be the best reduction method over the other methods.

2.4 Methods for Comparing Data

The most vital characteristic of modal testing is a comparison between the computed dynamic properties and those actually observed in practice (Ewins, 1995; Marwala, 1997; Ewins, 2001). This procedure is frequently called “validating” a theoretical model and it involves a number of stages. The first stage is to compare the specific dynamic properties, as measured against the predicted ones. The second stage is to measure the degree of the discrepancies or similarities between the two sets of data. The third stage is to bring the theoretical model closer to the measured data. When this is accomplished, the theoretical model is said to have been *updated*. In this section we closely study the computational methods used in the first, second and third stages.

In most situations, much endeavor goes into deriving the theory-based model and the experimentally derived model. For this reason, it is prudent to compare on as many different levels as possible. The dynamic model of a structure may be classified into *spatial*, *modal*, and *response* models (Ewins, 2001).

It is, at this time, appropriate to revisit this classification and attempt to compare the experimental and the theoretical model at each of these classifications. Consequently, a comparison of response properties as well as modal properties will be made. Comparisons between spatial properties are complex and, for that reason, will not be reflected on. In using any medium of comparison, the model must be developed comprehensively from the original form.

2.4.1 Direct Comparison

A) Comparisons of Natural Frequencies

The simplest method of comparison between the experimental and theoretical model is by comparing the natural frequencies (Ewins, 2001). This may be achieved by tabulating the experimental and theoretical natural frequencies. The most convenient way of comparison is to plot the graph of the experimental natural frequencies against the analytical ones for all available modes. If the gradient of the best straight line passing through the points is close to zero, then the correlation between the experimental and computed model is good. If the points lie spread out extensively about a straight line, then there is a severe failure of the model in representing the theoretical model’s capacity to estimate the measured natural frequencies and, therefore, the theoretical model should be re-evaluated. If the positions diverge to some extent from the straight line, in a systematic fashion, this implies that there is a particular characteristic responsible for the deviation.

B) Comparisons of Mode Shapes

The mode shapes can also be compared by plotting the analytical modes against the experimental ones. For a simple structure with well-separated modes, this technique of comparison may be used with ease. Nevertheless, for a complicated structure with modes that are close to one another, this technique frequently becomes tricky to employ. Therefore, it is appropriate to make comparisons of mode shapes at the same time as those of the natural frequencies.

In the situation where we have more data to handle for each mode, the comparison may be conducted by plotting the deformed shape for each model, experimental and theoretical, and overlaying one plot on the other. The disadvantage of this technique is that, even though the difference is evident, the plots are not easy to understand and they are usually confusing because there is so much information. A suitable method of comparison, which is along the lines of the natural-frequency plot, is to plot each element in the mode shape vector, experimental and theoretical, on an x - y plot (Ewins, 2001).

The individual points on this graph relate to modal coordinates, and it is expected that they should lie close to a straight line. If the mode shape vectors are mass-normalized, this straight line should have a slope of 1. If the points lie close to a straight line with a slope that is not 1, then one of the mode shapes is not mass-normalized *or* there is scaling error in the data. If the points are widely spread out about the line, then there is inaccuracy in one set or the other set. If the dispersion is too great, then it may be that the eigenvectors that are being compared do not relate to the same mode.

The slope of the best straight line is called the modal scale factor (MSF) and is defined as (Ewins, 2001):

$$MSF(\phi_a, \phi_m) = \frac{\{\phi_a\}^T \{\phi_m\}^*}{\{\phi_a\}^T \{\phi_a\}^*} \quad (2.23)$$

Here, ϕ_a is the analytical modes; ϕ_m is the measured modes; and $*$ is the complex conjugate.

The MSF parameter gives no indication of the quality of the measured points with respect to the straight-line fit.

2.4.2 Frequency-response Functions Assurance Criterion (FRFAC)

The benefit of using frequency-response functions (FRFs) straightforwardly is that they are measured directly. The easiest approach through which measured FRFs may be compared to the computed FRFs is by plotting the measured and theoretical FRFs in one plot (Ewins, 2001).

There are many measurements to be compared for particular FRF measurements. So, it becomes necessary to introduce a scalar factor (FRFAC) that gives the correlation between the measured and theoretical FRFs. One such scalar

factor uses the measured FRFs directly (Marwala, 1997) and can be written as follows:

$$FRFAC = \frac{\sum_{j=1}^M \sum_{n=1}^N |H_a(n, j)|}{\sum_{j=1}^M \sum_{n=1}^N |H_m(n, j)|} \quad (2.24)$$

Here, N is the number of degrees of freedom; M is the number of the measured frequency; H_m is the measured FRF; and H_a is the analytical FRF.

An FRFAC of 1 indicates that the measured FRFs perfectly reflect the analytical FRFs; the FRFAC that is greater than 1 indicate that the magnitude of the analytical FRFs is, on average, greater than the experimental ones. An FRFAC that is less than 1 indicates that the magnitudes of the experimental FRFs are, on average, greater than the analytical ones.

2.4.3 The Model Assurance Criterion (MAC)

The modal assurance criterion (MAC) compares the measured and the computed mode shapes. Stetson (2008) calculated the MAC from electronic holography data, while Allemang (2003) reviewed the use of the modal assurance criterion over a period of 20 years. Yuan *et al.* (2009a) used the MAC optimally place a sensor on a cable-stayed bridge, whereas Caponero *et al.* (2002) used an interferometer and the MAC for identification of component modes. Brechlin *et al.* (1998) introduced the scaled modal assurance criterion to analyze a system with rotational degrees of freedom, whereas Lars (1998) used the modal assurance criteria to analyze two orthogonal modal vectors. Finally, Desforges *et al.* (1996) used the MAC for tracking modes during flutter testing while Heylen and Janter (1989) applied the modal assurance criterion for dynamic model updating. The MAC can be mathematically summarized by the following equation (Allemang and Brown, 1982):

$$MAC_{cdr} = \frac{|\{\phi_{cr}\} \{\phi_{dr}^*\}|^2}{\{\phi_{cr}\}^T \{\phi_{cr}^*\} \{\phi_{dr}\}^T \{\phi_{dr}^*\}} \quad (2.25)$$

Here, MAC is modal assurance criterion; c is for reference; d is the degrees-of-freedom; r is the mode; T is the transpose; $*$ is the complex conjugate; and $\{\}$ is a vector.

The MAC is a measure of the least-squares deviation of the points from a straight-line correlation. A value close to 1 suggests that the two mode shapes are well correlated, while a value close to 0 indicates that the mode shapes are not correlated.

2.4.4 The Coordinate Modal Assurance Criterion (COMAC)

The COMAC technique is based on the same principle as the MAC and is, in essence, a measure of the correlation between the measured and the computed mode shapes for a given common coordinate. Meo and Zumpano (2008) used the COMAC for damage estimation on plate structures, while Zhao and DeWolf (2007) applied the COMAC for damage detection in a cracked I-shaped steel beam. The COMAC for coordinate j is given by (Lieven and Ewins, 1988):

$$COMAC(j) = \frac{\left(\sum_{r=1}^L |{}^j\phi_{ar} {}^j\phi_{mr}^*| \right)^2}{\sum_{r=1}^L ({}^j\phi_{ar})^2 \sum_{r=1}^L ({}^j\phi_{mr}^*)^2} \quad (2.26)$$

Unlike the MAC, the COMAC does not have any difficulty in comparing modes that are close in frequency or that are measured at insufficient transducer locations. L is the total number of well-correlated modes as indicated by the MAC. A value close to 1 suggests a good correlation. If the mode shape vectors are used then the COMAC becomes a vector. In this chapter, the MAC and direct comparison of mode natural frequencies are used to evaluate the effectiveness of the finite-element-model updating.

2.5 Optimization Methods

2.5.1 Nelder–Mead Simplex Method

The Nelder–Mead (NM) simplex method is one of the most used, direct optimization methods. First, the algorithm generates a simplex having $N+1$ vertices (x_i) in an N -dimensional space. Zhao *et al.* (2009) applied a modified NM simplex search for unconstrained optimization. The results obtained showed that the modified technique performs better than the original NM optimization method. Coelho and Araujo (2009) applied the NM simplex method for the successful identification in a Hénon chaotic map, while Ouria and Toufigh (2009) applied it for solving unconfined seepage problems.

Kalantar and Zimmer (2009) used the NM simplex method for optimally localizing vehicle formations, whereas Mastorakis (2009) applied this technique, finite-element modeling and a genetic algorithm for solving the Schrodinger–Maxwell's equations. Jung and Kim (2009) applied a hybrid of genetic algorithm and the NM simplex method for finite-element updating in a numerical bridge model.

A simplex of a specific dimension (a) is initialized around x_o using the following rule (Luersen and Riche, 2004; Ransome, 2006):

$$x_i = x_0 + \frac{a}{n\sqrt{2}}(\sqrt{n+1} + n - 1)e_i + \sum_{k=1 \neq i}^n \left[\frac{a}{n\sqrt{2}}(\sqrt{n+1} - 1) \right] e_k, i = 1, n \quad (2.27)$$

Here, e is the unit base vector.

The simplex vertices coordinates are changed through using the reflection, expansion and contraction operators. The procedure is explained as follows (Ransome, 2006):

- for a given iteration in the optimization procedure the vertex with the worst fitness measure as defined by Equation 2.4 is substituted by a new vertex;
- the coordinates of the new vertex are established by reflecting the old vertex's point about the outstanding vertices. An easy reflection of a two-dimensional simplex is illustrated in Figure 2.1;
- if the fitness measure of the current vertices is lower than the preceding removed vertex's fitness, the dimensions of the simplex are minimized and if not, it is enlarged; and
- this process is continued until the functional evaluation values of the vertices converge.

The convergence process is measured using the following inequality:

$$\sqrt{\sum_{i=1}^{n+1} \frac{(f_i - \bar{f})^2}{n}} < \tau \quad (2.28)$$

where τ is a small positive scalar and is computed by using:

$$\bar{f} = \frac{1}{n+1} \sum_{i=1}^{n+1} f_i \quad (2.29)$$

The advantages of the NM simplex method are (Bürmen *et al.*, 2006):

- it normally yields major progress in the initial iterations and rapidly gives acceptable results;
- it usually involves a single or double functional evaluation per iteration, apart from a shrink transformation;
- it succeeds in getting an excellent decrease in the function value by using comparatively few function evaluations; and
- it is simple to comprehend and use.

The disadvantages of the NM simplex are (McKinnon, 1998):

- it lacks a convergence theory;
- it experiences numerical failure even for smooth functions;

- it takes many iterations with insignificant improvement in the function value even when it is far from a minimum; and
- it experiences untimely convergence.

2.5.2 Quasi-Newton Broyden–Fletcher–Goldfarb–Shanno (BFGS) Algorithm

The quasi-Newton optimization method is a successful, robust and quadratically convergent optimization method that uses a gradient. The technique is a derivation of the Newton–Raphson method, with the difference being that the inverse of the second derivative is updated through using a one-dimensional or multi-dimensional Hessian estimation method. Ghosal and Chaki (2009) used the quasi-Newton method for estimating and optimizing the depth of penetration in CO₂ Laser-MIG welding. The Newton–Raphson algorithm is mathematically represented as follows (Ransome, 2006):

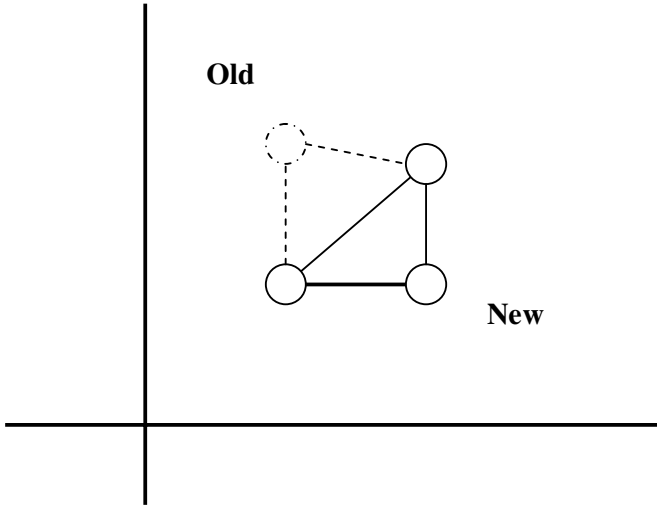


Figure 2.1 An easy reflection of a two-dimensional Simplex (Ransome, 2006)

$$x_{n+1} = x_n - \eta \frac{\dot{f}(x_n)}{\ddot{f}(x_n)} \quad (2.30)$$

Here, $f(x_n)$ is the objective function; and $\dot{f}(x_n)$ is the Jacobian (first-derivative), and $\ddot{f}(x_n)$ is the Hessian (second-derivative).

For a single-dimensional function, $\ddot{f}(x_n)$ can be updated by using the following equation:

$$\ddot{f}(x_{n+1}) = s_n / y_n \quad (2.31)$$

where

$$s_n = x_{n+1} - x_n \quad (2.32)$$

$$q_n = \dot{f}(x_{n+1}) - \dot{f}(x_n) \quad (2.33)$$

The most popular multi-dimensional technique for estimating the Hessian is the Broyden–Fletcher–Goldfarb–Shanno (BFGS) technique (Broyden, 1970; Fletcher, 1970; Goldfarb, 1970; Shanno, 1970). Sun *et al.* (2009) applied the BFGS technique for optimizing a machining allowance. Tan *et al.* (2009) applied the BFGS method for Stokes flows with fixed or moving interfaces and rigid boundaries, while Du *et al.* (2009) applied the BFGS method for optimizing the distribution of fibrous insulation. Further applications of the BFGS method include studies in aerodynamics (Papadimitriou and Giannakoglou, 2009), in solving equations (Yuan *et al.*, 2009b) and in nonconvex problems (Xiao *et al.*, 2009). The BFGS estimation of the inverse Hessian H_{n+1} is given by:

$$H_{n+1} = H_n + \frac{q_n q_n^T}{q_n^T s_n} - \frac{H_n^T s_n^T s_n H_n}{s_n^T H_n s_n} \quad (2.34)$$

From an initially estimated x_0 and Hessian matrix, H_0 , repeat the following steps (Nocedal and Wright, 2006):

1. Obtain a step s_n by solving $s_n = -H_n^{-1} \nabla f(x_n)$ and do a line search to discover an optimal step size λ_n in the direction obtained in the initial step, and then update $x_{n+1} = x_n + \lambda_n s_n$;
2. $q_n = \nabla f(x_{n+1}) - \nabla f(x_n)$;
3. Calculate the $H_{n+1} = H_n + \frac{q_n q_n^T}{q_n^T s_n} - \frac{H_n^T s_n^T s_n H_n}{s_n^T H_n s_n}$.

2.6 Example 1: Simple Beam

The aluminum beam shown in Figure 2.2 was used to test the NM simplex method and the BFGS method for finite-element-model updating. This beam had the following dimensions: length: 1.1 m, width: 29.2 mm and thickness: 9.6 mm. This beam had holes of diameters 5.8 mm located at the centers of elements 2 to 9 and, therefore, was difficult to model. Further details of this beam are reported by Marwala (1997). The beam was tested freely suspended using elastic rubber bands. The beam was excited using an electromagnetic shaker and the response was measured using an accelerometer. The beam was also modeled using the structural dynamics toolbox (Balmès, 1997) and it was divided into 11 elements. The finite-element model used Euler–Bernoulli beam elements (Zienkiewicz, 1971). It was excited at a position indicated by the double arrows and acceleration was measured at 10 positions indicated by the single arrows in Figure 2.2. A set of 10 frequency response functions were calculated and a roving accelerometer was used for testing. The moduli of elasticity of these elements were used as updating parameters. When the finite-element-model updating was implemented, the moduli of elasticity were restricted to vary from 6×10^{10} to 8×10^{10} N m⁻². The NM simplex optimization method and the BFGS were run to optimize Equation 2.4 and the results in Table 2.1 were obtained.

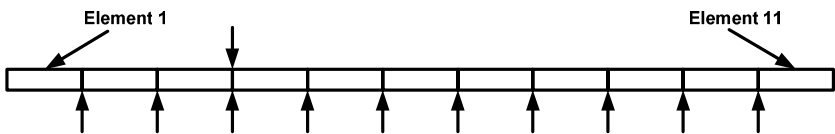


Figure 2.2 A beam with holes that is tested freely suspended

Table 2.1 Results showing measured frequencies of the beam, the initial frequencies and the frequencies obtained when the finite-element model of a beam is updated using the NM and BFGS

Modes	Measured frequency (Hz)	Initial frequency (Hz)	Frequencies from the NM updated model (Hz)	Frequencies from the BFGS updated model (Hz)
1	41.5	42.3	40.1	42.1
2	114.5	117.0	114.9	113.4
3	224.5	227.3	222.0	219.7
4	371.6	376.9	371.1	373.9

When a modulus of elasticity of 7×10^{10} N m⁻² was assumed, the error between the first measured natural frequency and that from the initial finite-element model was 1.9%. When the NM was used for finite-element-model updating, this error was increased to 3.4% but using BFGS reduced it to only 1.4%.

The error between the second measured natural frequency and that from the initial model was 2.2%. When the NM was used, this error was reduced to 0.3% while using BFGS reduced it to 1.0%.

The error of the third natural frequency between the measured data and the initial finite-element model was 1.2%. When the NM was used, this error was reduced to 1.1%, while using the BFGS reduced it to 2.1%.

The error between the fourth measured natural frequency and that from the initial model was 1.4%. When the NM was used for finite-element-model updating, this error was reduced to 0.1%, while using the BFGS reduced it to 0.6%. Overall, the NM gave the best results.

The updated models were also validated on the mode shapes they predicted. To make this assessment possible, the modal assurance criterion (MAC) was used (Allemang and Brown, 1983). The mean of the diagonal of the MAC vector was used to compare the mode shapes predicted by the updated and initial finite-element models to the measured mode shapes. The average MAC calculated between the mode shapes from an initial finite-element model and the measured mode shapes was 0.9986. When the average MAC was calculated between the measured data and data obtained from the updated finite-element models, the results in Table 2.2 were obtained.

Table 2.2 Beam results showing the MAC calculated between measured mode shapes and the initial finite-element model for the NM and BFGS updated finite-element model

Method	MAC
Initial model	0.9986
NM	0.9988
BFGS	0.9986

It is observed that only the NM updated finite model gave improved averages for the diagonals of the MAC matrix. The computational time taken to run the complete NM method was 20 CPU sec, while the BFGS took 21 CPU min to run. In conclusion, the NM method was found to be better than the BFGS method. This is mainly because the implementation of the BFGS method experienced many numerical problems due to the difficulty in estimating the gradient and the Hessian matrix. This, in a way, suggests that in implementing computational methods, gradient-based methods should be avoided for finite-element-updating methods.

2.7 Example 2: Unsymmetrical H-shaped Structure

The unsymmetrical H-shaped aluminum structure shown in Figure 2.3 was also used to validate the proposed method (Marwala, 1997). This structure had three thin cuts of 1 mm that went half-way through the cross-section of the beam. These cuts were introduced to elements 3, 4 and 5. The structure with these cuts was used so that the initial FE model gave data that were far from the measured data and, thereby, tested the proposed procedure with a difficult finite-element-model updating problem. The structure was suspended using elastic rubber bands. It was excited using an electromagnetic shaker and the response was measured using an accelerometer. The structure was divided into 12 elements. It was excited at the position indicated by the double arrows in Figure 2.3, and the acceleration was

measured at 15 positions indicated by the single arrows in Figure 2.3. The structure was tested freely suspended, and a set of 15 frequency-response functions were calculated. A roving accelerometer was used for measuring the response.

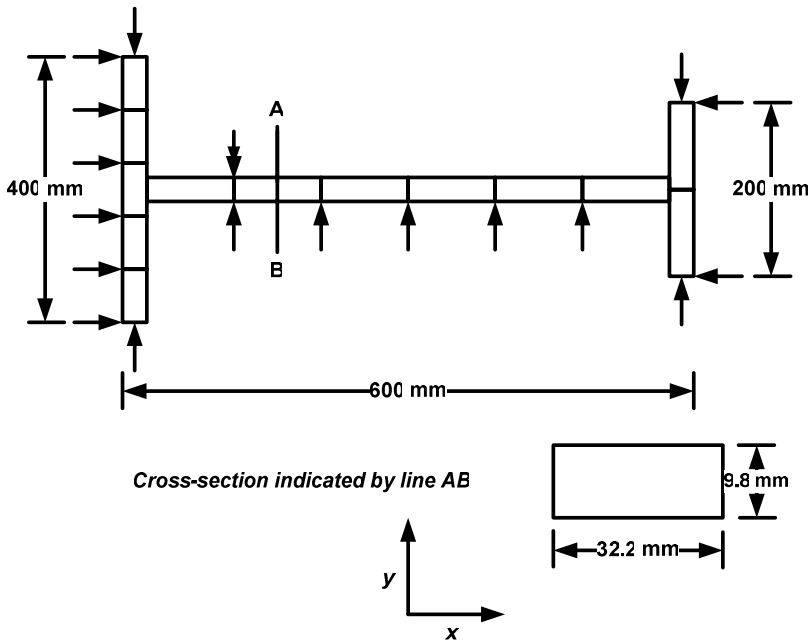


Figure 2.3 The irregular H-shaped structure

The mass of the accelerometer was found to be negligible compared to the mass of the structure. As in the previous example, the finite-element model was constructed using the structural dynamics toolbox (Balmès, 1997) with the Euler–Bernoulli beam elements (Zienkiewicz, 1971). The finite-element model contained 12 elements. The finite-element model of the structure contained 12 elements. As in the previous example, the moduli of elasticity of these elements were used as updating parameters, which were restricted to fall in the interval 6×10^{10} to $8 \times 10^{10} \text{ N m}^{-2}$. The NM and BFGS were implemented as in the previous example.

These optimization methods were implemented for finite-element-model updating, and the results obtained are shown in Tables 2.3 and 2.4. Table 2.3 shows the measured natural frequencies, initial natural frequencies and natural frequencies obtained by the NM and BFGS updated finite-element models. When a modulus of elasticity of $7 \times 10^{10} \text{ N m}^{-2}$ was assumed, the error between the first measured natural frequency and that from the initial finite-element model was 4.3%. When the NM was used for finite-element-model updating, this error was reduced to 1.1% and the BFGS approach reduced this error to 2.6%.

The error between the second measured natural frequency and that from the initial model was 8.4%. When the NM was used, this error was reduced to 1.4% and the BFGS reduced this error to 5.8%.

The error of the third natural frequencies between the measured data and the initial finite-element model was 9.6%. When the NM was used, this error was reduced to 2.4% and in using the BFGS it was reduced to 1.2%.

The error between the fourth measured natural frequency and that from the initial model was 3.7%. When the NM was used, this error was reduced to 0.7% and using the BFGS it was reduced to 2.1%.

The error between the fifth measured natural frequency and that from the initial model was 1.6%. When the NM was used this error was reduced to 2.6% and the BFGS reduced it to 1.1%.

Overall, the NM gave the best results with an average error calculated over all the five natural frequencies of 2.1%, while the BFGS gave an average error of 2.6%. On average, all four methods improved when compared to the average error between the initial finite-element model and the natural frequencies, which was 5.5%.

Table 2.3 Results from an unsymmetrical H-shaped structure showing measured frequencies, the initial frequencies and the frequencies obtained when the finite-element model was updated using the NM and BFGS

Modes	Measured frequency (Hz)	Initial frequency (Hz)	Frequencies from the NM updated model (Hz)	Frequencies from the BFGS updated model (Hz)
1	53.9	56.2	53.3	55.3
2	117.3	127.1	118.9	124.1
3	208.4	228.4	213.3	205.8
4	254.0	263.4	252.3	248.6
5	445.1	452.4	433.7	440.4

As in the previous example, the updated models implemented were validated on the mode shapes they predicted using the MAC. The NM- and BFGS-updated finite-element models gave improved averages for the diagonals of the MAC matrices of 0.8404 and 0.8403, respectively. When the computational load for each method was monitored, it was observed that, on average, the NM was the most computationally efficient method.

Table 2.4 Beam results showing the MAC calculated between measured mode shapes and the initial finite-element model for the NM and BFGS updated finite-element model

Method	MAC
Initial model	0.8394
NM	0.8404
BFGS	0.8403

Again, the results indicate that the NM method is marginally better than the BFGS method. The reason for this seems to be the fact that the calculations of the gradient and the Hessian matrix were fraught with numerical difficulties.

2.8 Conclusion

In this chapter the NM simplex and the BFGS methods were implemented for finite-element-model updating. When these techniques were tested on a simple beam and an unsymmetrical H-shaped structure, it was observed, on average, that the NM simplex method gave more accurate results than the BFGS method. This is mainly because the BFGS methods require the calculation of gradients, which is fraught with numerical errors. Furthermore, the NM method was found to be more computationally efficient than the BFGS method. For further work, hybrid techniques should be explored.

2.9 Further Work

This chapter compared the Nelder–Mead simplex and the BFGS methods for finite-element-model updating. These methods are classified as local search methods. For future work, other local search methods such as conjugate gradient method and the Levenberg–Marquardt algorithm need to be implemented for finite-element-model updating. In particular, their convergence properties within the context of finite-element-model updating also need to be studied. Further work should also include hybridizing these local search methods.

References

- Allemang RJ (2003) The Modal Assurance Criterion – Twenty Years of Use and Abuse. *Sound and Vib* 37:14–21
- Allemang RJ, Brown DL (1982) A Correlation Co-efficient for Modal Vector Analysis. In: *Proc of the 1st Int Modal Anal Conf*:01–18
- Azizi SM, Fekri MZ, Yazdani D, Bakhshai (2005), A. A BFGS-Based Method for Designing a Decentralized LQ Controller for Industrial Robot Manipulators. In: *Proc of the IEEE Conf on Control Appl*: 1558–1562
- Balmès E (1997) *Structural Dynamics Toolbox User's Manual*. Sci Softw Group Sèvres Fr Ver 2.1
- Bouhaddi N, Fillod R (1992) A Method for Selecting Master DOF in Dynamic Substructuring Using the Guyan Condensation Method. *Comput & Struct* 45: 941–946
- Brechlin E, Bendel K, Keiper W (1998) New Scaled Modal Assurance Criterion for Eigenmodes Containing Rotational Degrees of Freedom. In: *Proc of the 23rd Intl Conf on Vib Eng ISMA*:465–471
- Broyden CG (1970) The Convergence of a Class of Double-rank Minimization Algorithms. *J of the Inst of Math and its Appl* 6:76–90

- Bürmen A, Puhan J, Tuma T (2006) Grid Restrained Nelder-Mead Algorithm. *Comput Optim Appl* 34:359–375
- Bushard LB (1981) The Value of Guyan Reduction in Dynamic Thermal Problems. *Comp & Struct* 13:525–531
- Caponero MA, Paolozzi A, Peroni I (2002) Use of Speckle Interferometry and Modal Assurance Criterion for Identification of Component Modes. *Opt and Lasers in Eng* 37:355–367
- Coelho LdS, Araujo E (2009) Identification of the Hénon Chaotic Map by Fuzzy Modeling and Nelder-Mead Simplex Method. *Chaos, Solitons and Fractals* 41:2762–2772
- Corus M, Balmès E, Nicolas E (2006) Using Model Reduction and Data Expansion Techniques to Improve SDM. *Mech Res Commun* 35:398–407
- Das AS, Dutt JK (2008) Reduced Model of a Rotor-Shaft System Using Modified SEREP. *Mech Res Commun* 35:398–407
- Desforges MJ, Cooper JE, Wright JR (1996) Mode Tracking During Flutter Testing Using Modal Assurance Criterion. In *Proc of the Inst of Mech Eng J of Aerosp Eng* 210:27–37
- Du N, Fan J, Wu H, Sun W (2009) Optimal Porosity Distribution of Fibrous Insulation. *Intl J of Heat and Mass Transf* 52:4350–4357
- Ewins DJ (1995) *Modal Testing: Theory and Practice*. Research Studies Press, Letchworth
- Ewins DJ (2001) *Modal Testing: Theory, Practice and Application*. Mechanical Engineering Research Studies Engineering Dynamics Ser 2, Wiley
- Fletcher RA (1970) New Approach to Variable Metric Algorithms. *Compt J*. 13:317–322
- Friswell M I, Garvey SD, Penny JET (1995) Model Reduction Using Dynamic and Iterated IRS Techniques. *J of Sound and Vib* 186:311–323
- Friswell M I, Garvey SD, Penny JET (1998) The Convergence of the Iterated IRS Method. *J of Sound and Vib* 211:123–132
- Friswell MI, Mottershead JE (1995) *Finite Element Model Updating in Structural Dynamics*. Kluwer Academic Publishers Group, Norwell
- Fu ZF, He J (2001) *Modal Analysis*. Butterworth-Heinemann Publishers, Oxford
- Ghosal S, Chaki S (2009) Estimation and Optimization of Depth of Penetration in Hybrid CO2 LASER-MIG Welding using ANN-optimization Hybrid Model. *Intl J of Adv Manuf Technol*:01–9
- Guyan RJ (1965) Reduction of Stiffness and Mass Matrices. *AIAA J* 3:380
- Goldfarb DA (1970) Family of Variable Metric Updates Derived by Variational Means. *Math of Comput* 24:23–26
- Hägglblad RJ, Eriksson L (1993) Model Reduction Methods for Dynamic Analyses of Large Structures. *Comput & Struct* 47:735–749
- Heylen W, Janter T (1989) Applications of the Modal Assurance Criterion in Dynamic Model Updating. *Am Soc of Mech Eng, Des Eng Division DE* 18:289–294
- Jung DS, Kim CY (2009) FE Model Updating Based on Hybrid Genetic Algorithm and its Verification on Numerical Bridge Model. *Struc Eng and Mech* 32:667–683
- Kalantar S, Zimmer UR (2009) Optima Localization by Vehicle Formations Imitating the Nelder-Mead Simplex Algorithm. *Auton Robots*:01–22
- Kammer DC (2005) Sensor Set Expansion for Modal Vibration Testing. *Mech Syst and Signal Process* 19:700–713
- Kammer DC, Peck JA (2008) Mass-weighting Methods for Sensor Placement Using Sensor Set Expansion Techniques. *Mech Syst and Signal Process* 22:1515–1525
- Kim H, Cho M (2008) Sub-domain Reduction Method in Non-matched Interface Problems. *J of Mech Sci and Technol* 22:203–212
- Lars R (1998) Modal Assurance Criteria Value for Two Orthogonal Modal Vectors. In: *Proc of the Intl Modal Anal Conf – IMAC* 2:1320–1325

- Li H, Zhang M, Hu SJ (2008) Refinement of Reduced-models for Dynamic Systems. *Prog in Nat Sci* 18:993–997
- Lieven NAJ, Ewins DJ (1988) Spatial Correlation of Mode Shapes the Coordinate Modal Assurance Criterion (COMAC). In *Proc 6th Intl Modal Anal Conf*:690–695
- Luersen M, Riche RL (2004) Globalized Nelder-Mead Method for Engineering Optimization. *Comput & Struct* 82:2251–2260
- Marwala T (1997) A Multiple Criterion Updating Method for Damage Detection on Structures. Master's Thesis, University of Pretoria.
- Mastorakis NE (2009) Solution of the Schrodinger-Maxwell Equations via Finite Elements and Genetic Algorithms with Nelder-Mead. *WSEAS Trans on Math* 8:169–176
- McKinnon KIM (1998) Convergence of the Nelder-Mead Simplex Method to a Nonstationary Point. *SIAM J Optim* 9:148–158
- Meo M, Zumpano G (2008) Damage Assessment on Plate-like Structures Using a Global-Local Optimization Approach. *Optim and Eng* 9:161–177
- Nocedal J, Wright SJ (2006) *Numerical Optimization*. Springer-Verlag, Berlin
- Noor AK (1981) Recent Advances in Reduction Methods for Nonlinear Problems. *Comput & Struct* 13:31–44
- O'Callahan JC (1989) A Procedure for an Improved Reduced System (IRS) model. In: *Proc of the 7th Intl Modal Anal Conf*:29–37
- O'Callahan JC, Avitabile P, Riemer R (1989) System Equivalent Reduction Expansion Process. In: *Proc of the 7th Intl Modal Anal Conf*:29–37
- Olsson DM, Nelson LS (1975) The Nelder-Mead Simplex Procedure for Function Minimization. *Technometrics* 17:45–51
- Ouria A, Toufigh MM (2009) Application of Nelder-Mead Simplex Method for Unconfined Seepage Problems. *Appl Math Model* 33:3589–3598
- Papadimitriou DI, Giannakoglou KC (2009) The Continuous Direct-Adjoint Approach for Second Order Sensitivities in Viscous Aerodynamic Inverse Design Problems. *Comput and Fluids* 38:1539–1548
- Paz M (1984) Dynamic Condensation. *AIAA J* 22:724–727
- Paz M, Leigh W (2003) *Structural Dynamics: Theory and Computation*, Springer
- Prakash BG, Prabhu MSS (1986) Reduction Techniques in Dynamic Substructures for Large Problems. *Comput & Struct* 22:539–552
- Ransome TM (2006) Automatic Minimisation of Patient Setup Errors in Proton Beam Therapy. Master's Thesis, University of the Witwatersrand
- Salvini P, Vivio F (2007) Dynamic Reduction Strategies to Extend Modal Analysis Approach at Higher Frequencies. *Finite Elem in Anal and Des* 43:931–940
- Sastry CVS, Mahapatra DR, Gopalakrishnan S, Ramamurthy TS (2003) An Iterative System Equivalent Reduction Expansion Process for Extraction of High Frequency Response from Reduced Order Finite Element Model. *Comput Methods in Appl Mech and Eng* 192:1821–1840
- Shanno DF (1970) Conditioning of Quasi-Newton Methods for Function Minimization. *Math of Comput* 24:647–656
- Stetson KA (2008) Calculating Modal Assurance Criteria from Electronic Holography Data. *Sound and Vib* 42:06–11
- Sun YW, Xu JT, Guo DM, Jia ZY (2009) A Unified Localization Approach for Machining Allowance Optimization of Complex Curved Surfaces. *Precis Eng* 33:516–523
- Tan Z, Lim KM, Khoo BC (2009) An Immersed Interface Method for Stokes Flows with Fixed/Moving Interfaces and Rigid Boundaries. *J of Comput Phys* 228:6855–6881
- Xia Y, Lin R (2004) Improvement on the Iterated IRS Method for Structural Eigensolutions. *J of Sound and Vib* 270:713–727

- Xiao Y, Sun H, Wang Z (2009) A globally Convergent BFGS Method with Non-monotone Line Search for Non-convex Minimization. *J of Comput and Appl Math* 230:095–106
- Yang QW (2009) Model Reduction by Neumann Series Expansion. *Appl Math Modelling* 33:4431–4434
- Yin T, Lam HF, Chow HM, Zhu HP (2009) Dynamic Reduction-Based Structural Damage Detection of Transmission Tower Utilizing Ambient Vibration Data. *Eng Struct* 31:2009–2019
- Yuan A, Dai H, Sun D (2009a) Optimal Sensor Placement of Cable-Stayed Bridge Using Mixed Algorithm Based on Effective Independence and Modal Assurance Criterion Methods. *J of Vib, Measurement and Diagn* 29:U466
- Yuan G, Lu X, Wei Z (2009b) BFGS Trust-Region Method for Symmetric Nonlinear Equations. *J of Comput and Appl Math* 230:44–58
- Zhao J, DeWolf JT (2007) Modeling and Damage Detection for Cracked I-shaped Steel Beams. *Struct Eng and Mech* 25:131–146
- Zhao QH, Urošević D, Mladenović N, Hansen P (2009) A Restarted and Modified Simplex Search for Unconstrained Optimization. *Comput and Oper Res* 36:3263–3271
- Zienkiewicz OC (1971) *The Finite Element Method in Engineering Science*. McGraw-Hill, London

Finite Element Model Updating Using Computational
Intelligence Techniques

Applications to Structural Dynamics

Marwala, T.

2010, XV, 250 p., Hardcover

ISBN: 978-1-84996-322-0